Journal Pre-proof

Reprint of "Selective conversion of CO into ethanol on Cu(511) surface reconstructed from Cu(pc): Operando studies by electrochemical scanning tunneling microscopy, mass spectrometry, quartz crystal nanobalance, and infrared spectroscopy"

Jack H. Baricuatro, Youn-Geun Kim, Chu F. Tsang, Alnald C. Javier, Kyle D. Cummins, John C. Hemminger

PII: S1572-6657(20)30985-1

DOI: https://doi.org/10.1016/j.jelechem.2020.114757

Reference: JEAC 114757

To appear in: *Journal of Electroanalytical Chemistry*

Received date: 30 September 2019

Revised date: 20 November 2019

Accepted date: 26 November 2019

Please cite this article as: J.H. Baricuatro, Y.-G. Kim, C.F. Tsang, et al., Reprint of "Selective conversion of CO into ethanol on Cu(511) surface reconstructed from Cu(pc): Operando studies by electrochemical scanning tunneling microscopy, mass spectrometry, quartz crystal nanobalance, and infrared spectroscopy", *Journal of Electroanalytical Chemistry* (2019), https://doi.org/10.1016/j.jelechem.2020.114757

Contents lists available at ScienceDirect

Journal of Electroanalytical Chemistry

journal homepage: www.elsevier.com/locate/jelechem

Reprint of "Selective conversion of CO into ethanol on Cu(511) surface reconstructed from Cu(pc): *Operando* studies by electrochemical scanning tunneling microscopy, mass spectrometry, quartz crystal nanobalance, and infrared spectroscopy"☆

Jack H. Baricuatro [a,*], Youn-Geun Kim [a,*], Chu F. Tsang [a,b], Alnald C. Javier [a], Kyle D. Cummins [a], John C. Hemminger [b]

[a] Joint Center for Artificial Photosynthesis, Division of Chemistry and Chemical Engineering, California Institute of Technology, Pasadena, CA 91125, United States of America
[b] Department of Chemistry, University of California, Irvine, Irvine, CA 92697, United States of America

ARTICLE INFO

Article history:
Received 30 September 2019
Received in revised form 20 November 2019
Accepted 26 November 2019
Available online xxxx

Keywords:
Electrochemically generated Cu(511) surface
Operando electrode-surface microscopy
Operando molecular vibrational spectroscopy
CO adsorption on Cu vicinal surface
Selective reduction of CO into ethanol

ABSTRACT

A polycrystalline copper, surface-terminated by a well-defined (511)-oriented facet, was electrochemically generated by a series of step-wise surface reconstruction and iterations of mild oxidative-reductive processes in 0.1 M KOH. The electrochemical reduction of CO on the resultant stepped surface was investigated by four surface-sensitive *operando* methodologies: electrochemical scanning tunneling microscopy (STM), electrochemical quartz crystal nanobalance (EQCN), differential electrochemical mass spectrometry (DEMS), and polarization-modulation infrared spectroscopy (PMIRS). The stepped surface catalyzed the facile conversion of CO into ethanol, the exclusive alcohol product at a low overpotential of −1.0 *V* (SHE) or − 0.3 V (RHE). The chemisorption of CO was found to be a necessary prelude to ethanol production; i.e. the surface coverages, rather than solution concentrations, of CO and its surface-bound intermediates primarily dictate the reaction rates (current densities). Contrary to the expected predominance of undercoordinated step-site reactivity over the coordination chemistry of vicinal surfaces, vibrational spectroscopic evidence reveals the involvement of terrace-bound CO adsorbates during the multi-atomic transformations associated with the production of ethanol.

1. Introduction

Structure-composition-activity correlations are traditional guideposts in the rational discovery of catalysts. Systematic adherence to this tenet has ushered the synthesis of countless coordination compounds designed to fulfill elemental, electronic, and geometric prescriptions predicted to facilitate target reactions. Homogeneous catalysts active for CO_2 reduction (CO_2R), for instance, manifest high selectivities but only toward the production of carbon monoxide and formic acid in non-aqueous media [1,2]. In artificial photosynthesis that proceeds in water, only copper can sustain the multiple electron-transfer formation of C_1-C_2 products with appreciable reaction rates [3]. Specifically, at a potential of −1.45 *V* (SHE) and a current density of ca. 6 mA cm^{-2} [4], methane, ethylene, and ethanol have individual Faradaic efficiencies ≥10% [4]; these metrics, however, represent meager yields at the micromole scale during an hour-long polarization. Reaction kinetics at Cu electrodes can be enhanced at higher overpotentials although poor selectivity becomes the trade-off as evidenced by the emergence of fifteen CO_2R products [5]. A relatively narrow product distribution is offered by nickel at −1.40 *V* (SHE) and silver at −1.75 V (SHE) [4] but the dominance of hydrogen evolution reaction severely limits methanol and methane production to near trace-level concentrations.

An examination of the rich CO_2R literature uncovers the fact that the combination of Cu with other metals merely dilutes its inherent ability to catalyze CO_2R, once an accurate accounting of the electrochemically active surface area has been performed [6]. The distinctive electrocatalytic performance of Cu in its pristine state, therefore, provides impetus for the identification of the particular surface facet responsible for a preferred product or family of products. The endeavor is accomplished by the use of structurally well-defined electrodes prepared, treated, and analyzed according to the protocols of electrochemical surface science. Key events of heterogeneously

☆ A publisher's error resulted in this article appearing in the wrong issue. The article is reprinted here for the reader's convenience and for the continuity of the special issue. For citation purposes, please use the original publication details; Volume 857, 15 January 2020, 113704, DOI of original item: 10.1016/j.jelechem.2019.113704.
DOI of original article: http://dx.doi.org/10.1016/j.jelechem.2019.113704.

* Corresponding authors.
E-mail addresses: jackhess@caltech.edu, (J.H. Baricuatro), ygkim@caltech.edu. (Y.-G. Kim).

http://dx.doi.org/10.1016/j.jelechem.2020.114757

catalyzed reactions like the reduction of CO_2 and CO transpire at the electrical double layer developed at the electrode-electrolyte interface. Adsorbed reaction intermediates of the rate-determining and product-deciding steps are best studied by surface-sensitive techniques; processes at the fluxional diffusion layer, such as mass transport, do not alter the intrinsic catalytic activity but are subject to engineering controls for the performance optimization of CO_2R-based devices. Experimental data acquired from unambiguous surface structures are also invaluable to the calibration of theory-based mechanistic calculations.

The surface sensitivity of CO_2R on Cu electrocatalysts is demonstrated by the preferential formation, at low overpotentials, of methane on Cu (111) and ethylene on Cu(100) [6]. Product exclusivity is not fully realized at these low-index facets: At an onset potential of -1.39 *V* (SHE) in bicarbonate solution with a total current density of 5 mA cm^{-2}, Cu(100) catalyzes the CO_2-to-ethylene conversion at a Faradaic efficiency of 41% albeit with the non-negligible co-formation of methane, hydrogen, and C_2-C_3 alcohols [7]. Described in this report is the interfacial chemistry of an electrochemically generated stepped Cu surface that produces ethanol as the sole alcohol product from the reduction of CO. Unlike previous works that employ only pre-electrolysis characterization of vicinal single-crystal electrodes [7,8], the current investigation assembles *operando* methodologies that track the product composition, adlattice geometry, surface coverage, and surface coordination of adsorbates *during* the electroreduction of CO in alkaline solution. Present results are thus examined based on the atomic-level insights established earlier from the *seriatim* implementation of electrochemical scanning tunneling microscopy (STM), differential electrochemical mass spectrometry (DEMS), and quartz crystal nanobalance (EQCN). The strategic inclusion of electrochemical polarization-modulation infrared spectroscopy (PMIRS) now constitutes a *seriatim* quadruple combination of surface-sensitive techniques, STM-EQCN-DEMS-PMIRS, unprecedented in the conduct of CO reduction studies. The non-trivial consolidation of surface vibrational spectroscopy permits an examination of the role of terrace and step sites in the formation of C_2 products.

2. Materials and methods

Chemicals were used as received without further purification. All aqueous solutions were prepared using 18.2 MΩ-cm water (Barnstead Nanopure System). The blank solution was purged for at least 30 min in ultrahigh purity argon (Airgas, Radnor, PA). The alkaline electrolyte solution for the electrochemical reduction of CO consisted of freshly prepared 0.1 M KOH (99.99% pure, Sigma-Aldrich) bubbled for 30 min with high-purity (95%) carbon monoxide (Welding Supply Store, Duarte, CA).

All potentials were expressed in terms of the standard hydrogen electrode (SHE) scale. The equation $E_{SHE} = E_{RHE} - 0.059$ pH interconverts SHE and RHE, where RHE represents the reversible hydrogen electrode. Potentials on the SHE scale relate directly with thermodynamic free-energy changes such as $\Delta G^o = -nFE^o_{SHE}$, and are sensitive to changes in pH specifically for processes that involve the H^+/H_2 equilibrium.

The *operando* characterization of the Cu electrode via electrochemical scanning tunneling microscopy (STM) [9], electrochemical quartz crystal nanobalance (EQCN) [10], differential electrochemical mass spectrometry (DEMS) [11], and polarization-modulation infrared spectroscopy (PMIRS) [12] has been described previously at length. Only instrumental details pertinent to the investigation of the reconstruction phenomenon are summarized below.

Except for EQCN, all methods examined a polycrystalline Cu disk treated identically. The electrode (GoodFellow, Coraopolis, PA) was 99.99% pure Cu, 1.0 mm in thickness, and 10 mm in diameter. A mirror finish was achieved by metallographically polishing it in a suspension of polycrystalline diamond (Buhler, Lake Bluff, IL) at a grain size of 0.1 μm. The disk was rinsed with and sonicated in water, and then transferred to 85% H_3PO_4 for a 10-s electrochemical polish at 2.0 *V* using a 99.99% pure platinum wire (Goodfellow) counter electrode. The disk was further rinsed and thereafter covered with protective droplets of electrolyte prior to immediate use. A potential of -0.90 *V* (SHE) was applied for two hours to the Cu electrode while immersed in blank 0.1 M KOH to obtain Cu(pc)-[Cu(100)]. The reconstructed surface was subsequently cycled, at least 50 times between 0.1 V and $-$ 0.90 V, to generate Cu(pc)-[Cu(511)] [9,13].

Atomic details of the surface reconstruction of the copper electrode were tracked in 0.1 M KOH using a Nanoscope E microscope (Digital Instruments, Veeco, Santan Barbara, CA) that was refurbished (Advanced Surface Microscopy, Inc., Indianapolis, IN) and equipped with a three-electrode potentiostat. A Kel-F (Emco Industrial Plastics, Inc., Cedar Grove, NJ) electrochemical cell was specially built to accommodate the polycrystalline Cu disk working electrode; a miniature leakless Ag/AgCl (3.4 M KCl) reference electrode (Innovative Instruments, Inc., Tampa, FL); and a 99.99% pure Pt wire (Goodfellow) counter electrode. The STM tips were prepared from a tungsten wire (Sigma-Aldrich, St. Louis, MO), with a diameter of 0.25 mm, electrochemically etched in 1.0 M KOH at 15 *V*, AC. Transparent nail polish or Apiezon wax was used to coat the tip and minimize Faradaic currents. A high-resolution scanner in a constant-current mode was employed for image acquisition at the chosen potential. The images were not subjected to any post-scan processing such as the use of software transforms or high-pass filters.

Operando changes in the mass of the Cu electrode at the nanogram regime were measured by a Seiko-EG&G QCA922 analyzer (Bio-logic, Knoxville, TN) interfaced to a Bio-Logic SP-200 potentiostat. A specially constructed electrochemical cell [14] held ports for the introduction of CO into the solution and its headspace. Provisions were available for the insertion of a reversible hydrogen electrode (RHE) configured with a Luggin capillary that hovered close to the working electrode. The counter electrode was a coil of gold wire. An AT-cut quartz crystal, coated on both sides with approximately 300-nm thick polycrystalline Cu, served as the resonator-working electrode with a resonance frequency of 9 MHz. Potential-dependent adsorption measurements were acquired while the Cu electrode was in contact with CO-saturated 0.1 M KOH for at least 60 s. The same electrochemical protocol transacted for the Cu disk electrode (vide supra) was followed to create the Cu(pc)-[Cu(100)] and Cu(pc)-[Cu(511)] surfaces.

Mass spectrometric information during potentiostatic experiments was afforded by DEMS. A custom-built three-electrode electrochemical cell was employed in conjunction with an HPR-20 quadrupole mass spectrometer (Hiden Analytical, Warrington, England) equipped with a secondary electron multiplier detector set at 950 *V* with an emission current of 500 μA. The working electrode was a polycrystalline Cu disk; and the counter electrode, a 99.99% pure Pt wire (Goodfellow). The base peak of ethanol at $m/z = 31$, indicative of the resonance-stabilized $[CH_2OH]^+$ cation, is shared by other alcohols. Methanol does not register a peak at $m/z = 45$, which corresponds to the (M-1) oxonium ion species of ethanol formed from loss of a hydrogen radical adjacent to the hydroxyl group [15]. MS signals for ethanol were monitored at m/z = 31 and 45 but, in the established absence of methanol, only the former signal was reported due to its high signal-to-noise ratio.

Vibrational spectroscopic characterization of CO adsorbates at the electrode-electrolyte interface was conducted using a Nicolet 6700 FT-IR spectrometer (Thermo Electron Scientific, Madison, WI) connected to a Nicolet tabletop optical module (TOM). Nitrogen gas was constantly fed into the appended TOM to create a stable inert atmosphere for the optical elements, polarization modulator and demodulator, and the liquid-nitrogen-cooled narrow-band HgCdTe detector. The polarization state of the IR beam was rapidly switched at a modulation frequency of 50.047 kHz between the *s*- and *p*-states using a Hinds PEM-100 ZnSe photoelastic modulator (Hind Instruments, Portland, OR). A half-wave retardation setting of 2300 cm^{-1} was used to optimize signals at the CO frequency region without severe baseline distortions. The spectral plot is a ratio of the "Channel B" modulated signal intensities ($I_s - I_p$) divided by the "Channel A" unmodulated signal ($I_s + I_p$) generated by the GWC synchronous-sampling demodulator (GWC Instruments, Madison, WI). Electrochemical experiments were

performed using a custom-built Kel-F thin-layer electrochemical cell patterned from the design of Seki, et al. [16] which allowed the insertion of a miniature leakless Ag/AgCl (3.4 M KCl) reference electrode and a flame-annealed Pt wire counter electrode close to a Cu disk working electrode.

3. Results and discussion

The high mobility of the surface atoms of copper, evidenced by its relatively low cohesive energy compared to other lighter face-centered cubic transition metals located to its left in the periodic table [17], underpins the susceptibility of the polycrystalline surface to reconstruct in alkaline solutions under sufficiently negative potentials. The discovery of the Cu (pc) → Cu(pc)-[Cu(111)] → Cu(pc)-[Cu(100)] surface transformation [13], a process that transpires independent of electrolyte effects [18], allows the facile correlation of catalytic activity and selectivity with well-defined surface structures without the deployment of expensive bulk single crystals. The formation of low-index planes at electrochemical environments proximate to those during electrocatalysis is favorable especially for an oxophilic metal like Cu that readily captures sub-monolayer coverages of oxygen even at potentials over half-a-volt more negative than the open-circuit value.

The electrochemically prepared Cu(*hkl*) surfaces do not retain their monocrystallinity once the electrode is removed from the influence of the applied potential in solution; i.e. the surface becomes oxided and reverts to an ill-defined polycrystalline state. The predicament severely raises a caveat against the validity of ex situ and in situ characterization of copper in the context of the electrochemical reduction of CO_2. These observations underscore the importance of a finite interfacial energy [19] required to preserve the reconstructed layer that rests atop the unperturbed polycrystalline pedestal. Efforts to ascertain the thickness of the rearranged top layers using *operando* synchrotron-based XRD measurements are limited by the accessible grazing angle of incidence acute enough to probe exclusively the selvedge region. Thus far, the steepest angle afforded by the attempted experiments convolutes a 10-monolayer-deep structural information composite of the surface and subsurface regions.

The Cu(pc)-[Cu(100)] electrode can undergo further structural changes by steady-state cyclic voltammetry in contradistinction to the reconstruction-resistant behavior of the bulk Cu(100) crystal under similar conditions [20]. The structural evolution of Cu(pc) is summarized in Fig. 1A–E. The potential vertices of the cycles were − 0.90 *V* and 0.10 V. The values were chosen to minimize, but not totally exclude, effects from the hydrogen evolution reaction and the onset of Cu(I) oxide formation during the cathodic and anodic scans, respectively. The resultant surface consists of 3-atom wide (100) terraces bound by a (111)-oriented monoatomic step as revealed by the STM (Fig. 2A). The surface bears the step notation Cu(*S*)-[3(100) x (111)], which is succinctly denoted as Cu (511). The dihedral angle between normal planes of the (511) surface and its (100) terrace is 15.79°. Hence, the (100) terraces protrude like angled slats from the surface so that, when viewed at large magnification, the step edges of the terraces appear as a bright linear array and partly eclipse the corner atoms (Fig. 2B). The Cu(pc)-[Cu(511)] surface was observed at a narrow potential window between −0.90 *V* to −1.10 V; the sharpness of the STM images acquired during a potentiostatic hold at −1.10 V degraded quickly due to hydrogen evolution. At more negative potentials, the image was indecipherable; as the potential was switched back to −0.90 V, the same stepped structure can be recaptured. Widespread structural regularity can be achieved after 20 potential cycles between −0.90 V and 0.10 V, although wide variations in the initial state of polycrystalline Cu can prolong the time needed to achieve surface order. Unlike polycrystalline noble metals like Pt, Pd, and Au whose thermally annealed clean surfaces constitute reproducible initial states [21], Cu relies on subjective mechanical and electrochemical polishing protocols that inevitably shifts the timeframe to complete the multistep transition.

A few remarks are essential to understand the voltammetric scheme used to generate Cu(pc)-[Cu(511)]. Classic electrochemical procedures for the development of preferred crystallographic orientation on face-centered cubic metals employ rapid iterations, at a frequency of a few kHz, of electrodissolution and electrodeposition [22]. The present preparative route intentionally excludes the formation Cu(II) and its oxides and hydroxides, which are reported to redeposit copper as islands and nanostructured assemblies [23]. Despite claims of enhanced activity of CO_2 reduction on nanoparticles compared to foils, marginal differences exist when the geometric-area-based current densities are recalculated in terms of the electrochemically active surface area. Furthermore, the use of a wide potential window for the oxidation-reduction cycles can introduce traces of copper oxides that can *temporarily* persist during CO_2 reduction and alter the product profile *non-catalytically*; i.e. the oxides merely behave as reactants that, once consumed, cannot be regenerated under highly reductive conditions due to prohibitive thermodynamics.

The product distribution of the electrochemical reduction of CO in 0.1 M KOH at Cu(pc)-[Cu(511)] was assayed by differential electrochemical mass spectrometry (DEMS). The only product detected at −1.06 *V* was ethanol (Fig. 3), a potential that is 150 mV more positive than the onset of hydrocarbon production on Cu in basic medium. Neither the reconstructed Cu(pc)-[Cu(100)] surface nor the multiply cycled Cu(100) bulk electrode yielded ethanol and other CO-reduction products at the narrow potential window of interest [20]. The impact of this result rests on the identification of a well-defined *operando* surface structure of Cu responsible for the production of a singular alcohol. The product selectivity that favors alcohols over hydrocarbons is realized at low overpotentials at the expense of low current densities.

The DEMS ion-current signal for ethanol was superimposed with the potential-dependent surface coverage of CO at Cu(pc)-[Cu(511)] so that both traces share the same abscissa. Details of the construction of the CO surface coverage-vs-potential plots using electrochemical quartz crystal nanobalance (EQCN) were reported earlier [10]. Fig. 4 shows a drastic rise in the fractional surface coverage, θ_{CO}, from zero to 0.5 as the potential was stepped from −0.80 *V* to −0.85 V. UHV studies on the low-temperature adsorption of CO on Cu(100) surface indicated that, at

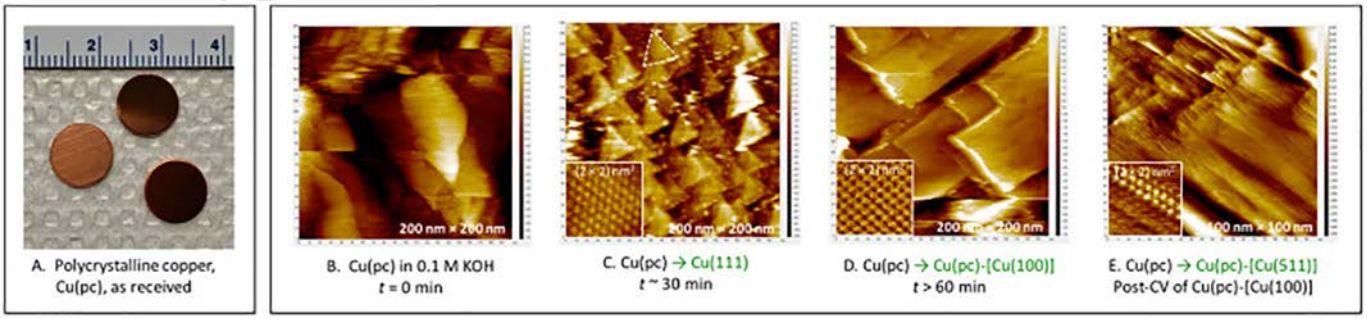

Fig. 1. A. Polycrystalline copper, Cu(pc), disk electrode. B. STM image of Cu(pc) surface at the start of polarization at E(SHE) = −0.90 *V* in 0.1 M KOH. C. Cu(pc) initially generates a (111)-oriented surface. D. Further surface reconstruction yields Cu(pc)-[Cu(100)]. E. Subsequent potential cycling of D between −0.90 V and 0.10 V in 0.1 M KOH gives rise to a stepped surface. Bias potential, E_{bias} = 250 mV. Tunneling current, I_t = 2 nA for wide-scale images; 5 nA for high-resolution images.

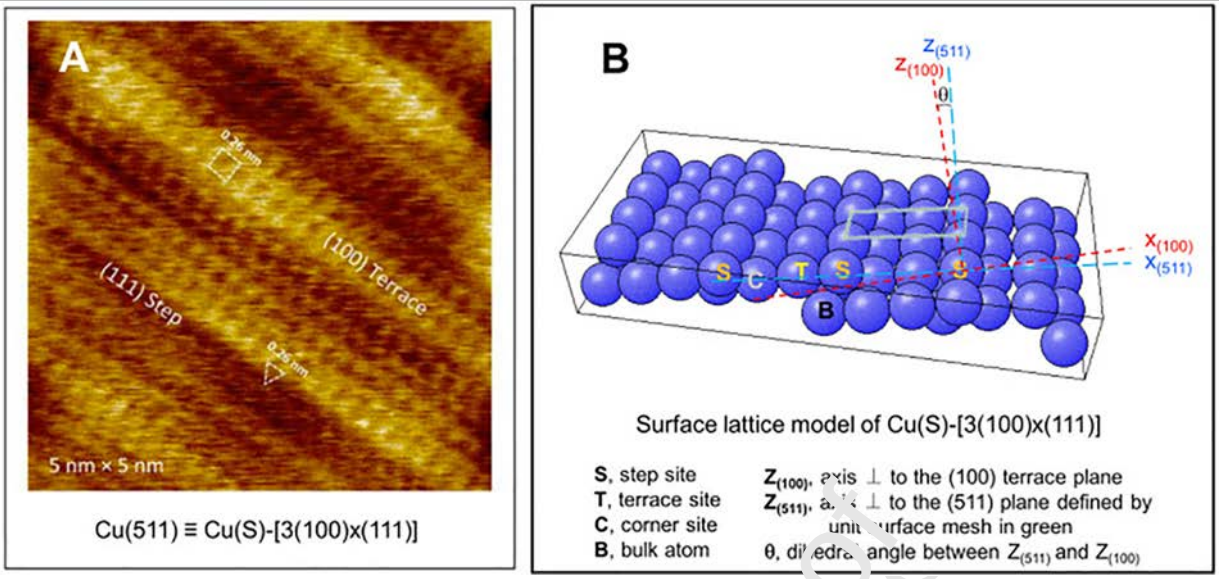

Fig. 2. A. High-resolution STM image of a Cu(511) surface shows (100) terrace planes, indicated by the square unit mesh, and monoatomic (111) steps delineated by a triangle. B. The step, terrace, and corner sites of an ideal Cu(*S*)-[3(100)x(111)] surface. A quarter of a surface atom is located at each corner of the rectangular unit surface mesh, in green, of Cu(511). (For interpretation of the references to colour in this figure legend, the reader is referred to the web version of this article.)

high-vacuum pressures, the surface already reaches saturation coverage at $\theta_{CO} = 0.5$, which corresponds to a $c(2 \times 2)$ adlattice [24]. The CO-to-based on the potential-dependence of the former and the invariance of the latter.

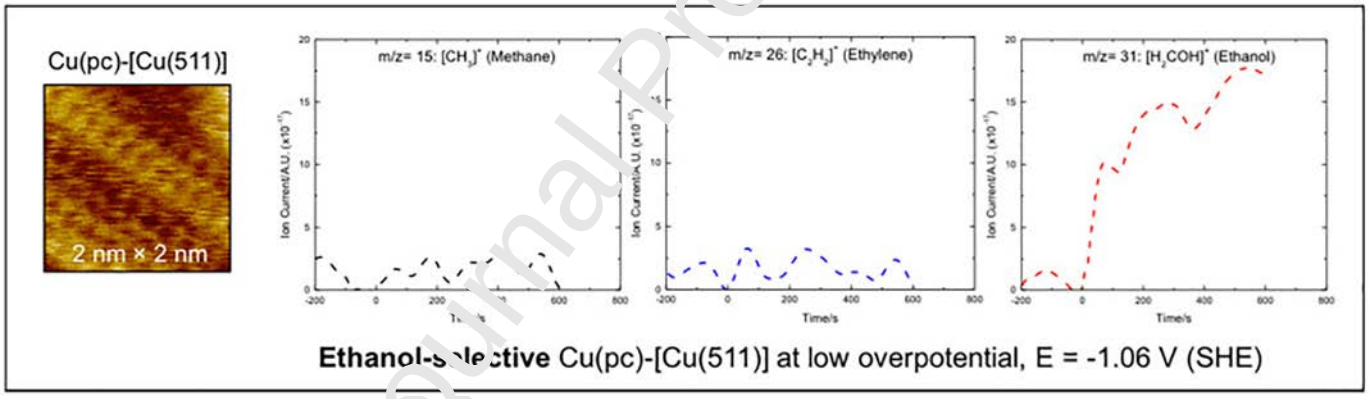

Fig. 3. Product analysis of the electrochemical reduction of CO at Cu(pc)-[Cu(511)] reveals ethanol as the only carbonaceous product. The DEMS signals for methane and ethylene were essentially zero at E(SHE) = −1.06 V in 0.1 M KOH.

ethanol conversion did not ensue until −1.06 V was reached; at this potential the surface was saturated with adsorbed CO. The concentration of CO dissolved in the electrolytic solution, previously bubbled with gaseous CO, was found sufficient to replenish any reacted CO within four hours of polarization in the low overpotential region.

The vibrational characteristics of the surface-confined CO molecules on Cu(pc)-[Cu(511)] were examined by polarization-modulation infrared spectroscopy. The high-frequency modulation between the *s*- and *p*-states of the infrared beam affords surface sensitivity to the technique: Only *p*-polarized beam can interact with adsorbates that have a net dipole moment perpendicular to the surface [25]. A plot of the ratio between the modulated and demodulated intensities as a function of wavenumber minimizes isotropic spectral contributions from solution species. Bands for the stretching, bending, and librating modes of water, for instance, are not completely removed because the distance between the electrode and CaF_2 window in the thin-layer cell configuration is of the same order of magnitude as the wavelength of the IR beam. PMIRS peaks from surface-bound and solution-based species can be discriminated

Fig. 5 shows the PMIRS spectra of CO adsorbed on Cu(pc)-[Cu(511)] in CO-saturated 0.1 M KOH. The presence of (100) terraces on the stepped surface warrants a comparison of the CO_{ads}-Cu(100) spectral signature discussed elsewhere [12]. The IR peak for CO on Cu(pc)-[Cu(511)] appeared in the same region as that for CO on Cu(100). The spectral resemblance at 2020 cm^{-1}–2030 cm^{-1} suggests the involvement of terrace-bound carbon atoms during the formation of ethanol. Such multi-atomic process is, hence, not exclusively confined at coordinatively unsaturated sites. A thorough analysis of the energy landscape that surrounds the geometric requirements for C_2 production on step-terrace ensembles is beyond the scope of the report.

Under electrochemical conditions, the surface-coordination site and vibrational characteristics of CO chemisorbed on Cu(pc)-[Cu(511)] are evidently different from those observed in vacuo for a family of stepped surfaces. Ultrahigh vacuum studies of the cryogenic chemisorption CO at the vicinal surfaces of Cu (211), (311), and (755) identify a singular IR band at 2090 cm^{-1}–2110 cm^{-1} ascribed to CO adsorbates on step sites [26]. Although the specific region appears active in the present

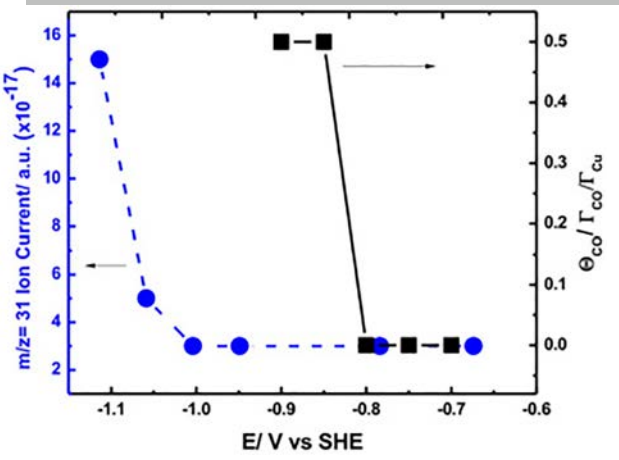

Fig. 4. Potential-dependent behavior of the ion current for the base peak of ethanol (m/z = 31) in blue and the fractional surface coverage, Θ, of CO at Cu(pc)-[Cu (511)] in black. The lines that interconnect the data points serve only as visual guide. (For interpretation of the references to colour in this figure legend, the reader is referred to the web version of this article.)

electrochemical PMIR spectra, the signal-to-noise does not permit an unambiguous step-specific peak assignment. The irresistible assertion that the barely discernible CO-on-step feature in PMIRS indicates a lower CO-adsorbate population on steps compared to that on terraces has to be avoided in view of the well-documented intensity borrowing phenomena of neighboring CO peaks on Cu surfaces; i.e. the absorption intensities do not necessarily scale linearly with the surface coverage of the IR-active absorber [27]. Essential to the elucidation of the potential-dependent spectroscopic features of CO during its electrochemical reduction at Cu surfaces is hinged on the full characterization of the nature of the bond between Cu and CO. A definitive description of the orbital picture during the Cu-CO formation specifically at the electrode-electrolyte interface has yet to be formulated. The metal-carbon bond is generally treated in terms of the classic Blyholder model [28] although the apparently restrictive closed *d*-shell configuration (s^1d^{10}) of Cu would have initially precluded the CO-to-metal electron donation prior to the metal-to-CO backdonation. Analysis of the X-ray emission spectra of the carbon and oxygen *K*-edges for CO adsorbed on Cu(100) has led to refinements of the Blyholder model that now considers 4σ-5σ orbital mixing and the hybridization of the whole π-electronic structure of CO instead of a purely frontier-orbital interaction [29]. The applicability of the updated Blyholder model to the surface bonding of CO on Cu remains untested under electrochemical conditions since present experimental evidences are acquired in ultrahigh vacuum.

4. Conclusion

A series of step-wise potential-dependent reconstruction transformed the surface of a polycrystalline Cu electrode exposed to alkaline solution into a well-defined Cu(*S*)-[3(100) x (111)] or (511) surface. Ethanol was the exclusive alcohol product at the stepped Cu surfaces at a low overpotential of −1.06 *V* (SHE); no hydrocarbons such as ethylene or methane were co-generated. The chemisorption of CO on Cu is a prerequisite for the transformation of CO into alcohols. Contrary to the expectation that undercoordinated (step) sites predominantly steer the overall reactivity of vicinal surfaces, vibrational spectroscopic evidence reveals the involvement of terrace-bound CO adsorbates in the production of ethanol.

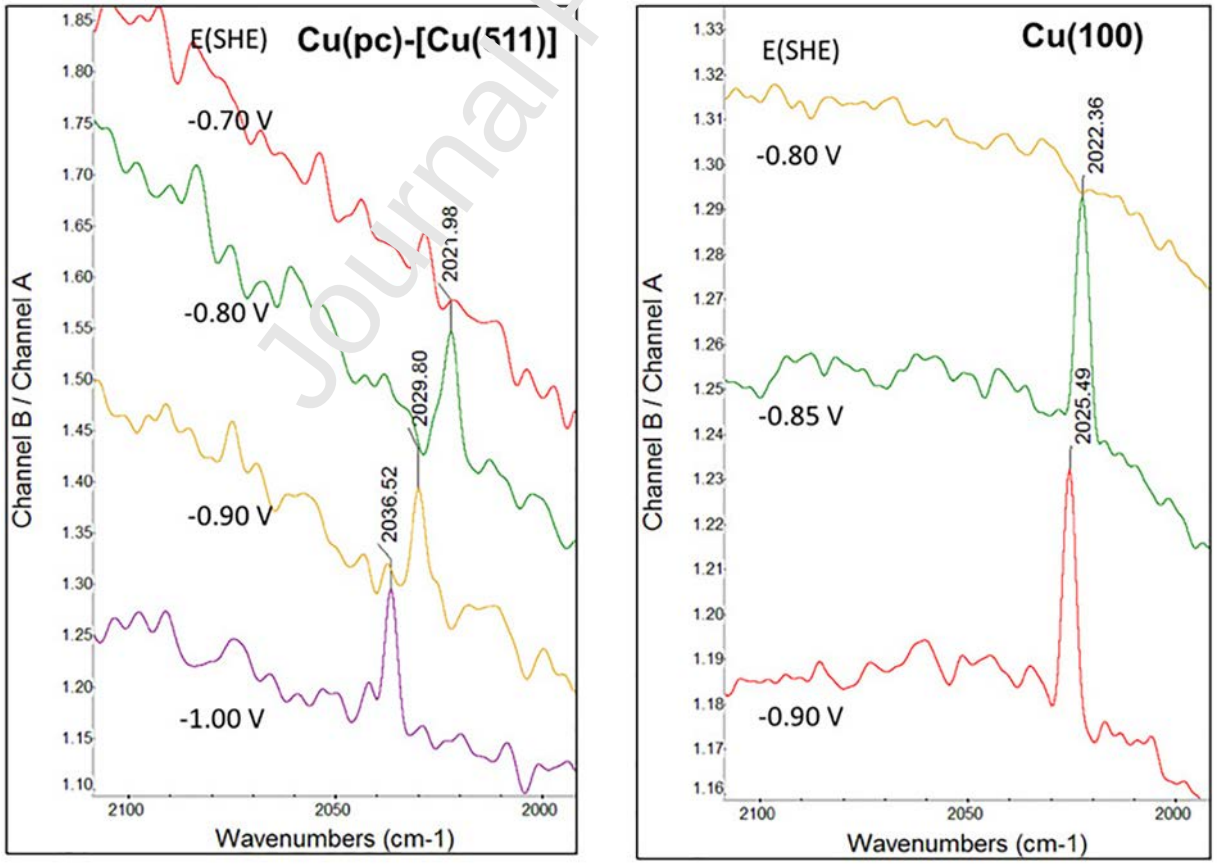

Fig. 5. The CO stretch frequency region in the polarization-modulation infrared spectra of *left panel*: the electrochemically generated Cu(pc)-[Cu(511)]; *right panel*: Cu(100) in CO-saturated 0.1 M KOH during potentiostatic experiments.

Authors contributions

J.H.B., Y.-G.K., C.F.T., A.C.J., K.D.C. and J.C.H. designed research
J.H.B., Y.-G.K., C.F.T., A.C.J., performed research
J.H.B., Y.-G.K., C.F.T., A.C.J., K.D.C. and J.C.H. analyzed data
J.H.B. wrote the paper

Declaration of interest

None.

Acknowledgment

This material is based upon work performed by the Joint Center for Artificial Photosynthesis, a DOE Energy Innovation Hub, supported through the Office of Science of the U.S. Department of Energy under Award No. DE-SC0004993.

References

[1] E.P. Benson, C.P. Kubiak, A.J. Sathrum, J.M. Smieja, Electrocatalytic and homogeneous approaches to conversion of CO_2 to liquid fuels, Chem. Soc. Rev. 38 (2009) 89–99.
[2] R. Francke, B. Schille, M. Roemelt, Homogeneously catalyzed electroreduction of carbon dioxide – methods, mechanisms, and catalysts, Chem. Rev. 118 (2018) 4631–4701.
[3] Y. Hori (Ed.), Handbook of Fuel Cells: Fundamentals, Technology and Application, 2, VHS-Wiley, Chichester 2003, pp. 720–733.
[4] K.P. Kuhl, T. Hatsukade, E.R. Cave, D.N. Abram, J. Kibsgaard, T.F. Jaramillo, Electrocatalytic conversion of carbon dioxide to methane and methanol on transition metal surfaces, J. Am. Chem. Soc. 136 (2014) 14107–14113.
[5] K.P. Kuhl, E.R. Cave, D.N. Abram, T.F. Jaramillo, New insights into the electrochemical reduction of carbon dioxide on metallic copper surface, Energy Environ. Sci. 5 (2012) 7050–7059.
[6] Y. Hori, "Electrochemical CO_2 reduction on metal electrodes", Modern Aspects of Electrochemistry, No. 42, C.G. Vayenas, R.E. White, M.E. Gamboa-Aldeco, Springer: New York p. 89–189.
[7] Y. Hori, I. Takahashi, O. Koga, N. Hoshi, Selective formation of C2 compounds from electrochemical reduction of CO_2 at a series of copper single crystal electrodes, J. Phys. Chem. B 106 (2002) 15–17.
[8] K.J.P. Schouten, E.P. Gallent, M.T.M. Koper, Structure sensitivity of the electrochemical reduction of carbon monoxide on copper single crystals, ACS Catal. 3 (2013) 1292–1295.
[9] Y.-G. Kim, A. Javier, J.H. Baricuatro, M.P. Soriaga, Regulating the product distribution of CO reduction by the atomic-level structural modification of the Cu electrode surface, Electrocatalysis 7 (2016) 391–399.
[10] C.F. Tsang, A.C. Javier, Y.-G. Kim, J.H. Baricuatro, K.D. Cummins, J. Kim, G. Jerkiewicz, J.C. Hemminger, M.P. Soriaga, Potential-dependent adsorption of CO and its low-overpotential reduction to CH_3CH_2OH on Cu(511) surface reconstructed from Cu(pc): operando studies by seriatim STM-EQCN-DEMS, J. Electrochem. Soc. 165 (2018) J3350–J3354.
[11] A. Javier, B. Chmielowiec, J. Sanabria-Chinchilla, Y.-G. Kim, J.H. Baricuatro, M.P. Soriaga, A DEMS study of the reduction of CO_2, CO, and HCHO pre-adsorbed on Cu electrodes: empirical inferences on the CO_2RR mechanism, Electrocatalysis 6 (2015) 127–131.
[12] J.H. Baricuatro, Y.-G. Kim, C.L. Korzeniewski, M.P. Soriaga, Seriatim ECSTM-ECPMIRS of the adsorption of carbon monoxide on Cu(100) in alkaline solution at CO_2-reduction potentials, Electrochem. Commun. 91 (2018) 1–4.
[13] Y.-G. Kim, J.H. Baricuatro, A. Javier, J.M. Gregoire, M.P. Soriaga, The evolution of the polycrystalline copper surface, first to Cu(111) and then to Cu(100), at a fixed CO_2RR potential: a study by operando EC-STM, Langmuir 30 (2014) 15053–15056.
[14] G. Jerkiewicz, G. Vatankhah, A. Zolfaghari, J. Lessard, Analysis of the mass response of the electrochemical quart-crystal nanobalance in horizontal and vertical geometry, Electrochem. Commun. 1 (1999) 419–424.
[15] J.H. Gross, Mass Spectrometry, Springer, New York, 2004 241.
[16] H. Seki, K. Kunimatsu, W. Golden, Appl. Spectrosc. 39 (1985) 437–443.
[17] H.P. Myers, Introductory Solid State Physics, 2nd ed Taylor & Francis, Philadelphia, 1997 15.
[18] Y.-G. Kim, J.H. Baricuatro, M.P. Soriaga, Surface reconstruction of polycrystalline Cu electrodes in aqueous $KHCO_3$ electrolyte at potentials in the early stages of CO_2 reduction, Electrocatalysis 9 (2018) 526–530.
[19] D.H. Buckley, Surface effects in Adhesion, Friction, Wear, and Lubrication, Elsevier, Amsterdam, 1981 270.
[20] Y.-G. Kim, A. Javier, J.H. Baricuatro, D. Torelli, K.D. Cummins, C.F. Tsang, J.C. Hemmingers, M.P. Soriaga, Surface reconstruction of pure-Cu single-crystal electrodes under CO-reduction potentials in alkaline solutions: a study by seriatim ECSTM-DEMS, J. Electroanal. Chem. 780 (2016) 290–295.
[21] K. Itaya, In situ scanning tunneling microscopy in electrolyte solutions, Prog. Surf. Sci. 58 (1998) 121–247.
[22] E.V. Albano, H.O. Martin, A.J. Arvia, A mechanistic model for the electrochemical faceting of metals with development of preferred crystallographic orientations, Electrochim. Acta 33 (1988) 271–277.
[23] S.Y. Lee, H. Jung, N.-K. Kim, H.-S. Oh, B.K. Min, Y.J. Hwang, Mixed copper states in anodized Cu electrocatalyst for stable and selective ethylene production from CO_2 reduction, J. Am. Chem. Soc. 140 (2018) 8681–8689.
[24] M.A. Chesters, J. Pritchard, LEED and surface potential study of carbon monoxide and xenon adsorbed on Cu(100), Surf. Sci. 28 (1971) 460–468.
[25] R.G. Greenler, Infrared study of adsorbed molecules on metal surfaces by reflection techniques, J. Chem. Phys. 44 (1966) 310–315.
[26] P. Hollins, J. Pritchard, Intermolecular interactions and the infrared reflection-absorption spectra of chemisorbed carbon monoxide on copper, in: A.T. Bell, M.L. Hair (Eds.), Vibrational Spectroscopies for Adsorbed Species ACS Symposium Series, American Chemical Society, Washington, DC 1980, pp. 51–73.
[27] E. Borguet, H.-L. Dai, Site-specific properties and dynamical dipole coupling of CO molecules adsorbed on vicinal Cu(100) surface, J. Chem. Phys. 101 (1994) 9080.
[28] G. Blyholder, Molecular orbital view of chemisorbed carbon monoxide, J. Phys. Chem. 68 (1964) 2772.
[29] A. Nilsson, L.G.M. Pettersson, J.K. Norskov, Chemical Bonding at Surfaces and Interfaces, Elsevier, Amsterdam, 2008.